Handout 9

Measurement of bandstructure

9.1 Introduction

This Lecture will describe a selection of the most common techniques used to measure the bandstructures of solids. Many of these techniques involve the use of magnetic fields to partially quantise the electronic motion; this is known as *Landau quantisation* or *cyclotron motion*. I shall therefore treat the motion of band electrons in some detail before giving brief details of the techniques themselves.

9.2 Lorentz force and orbits

9.2.1 General considerations

Equation 5.9 may be used to calculate the effect of an external magnetic field $\mathbf{B}$ on a band electron, *i.e.*

$$\hbar \frac{\mathrm{d}\mathbf{k}}{\mathrm{d}t} = -e\mathbf{v} \times \mathbf{B}, \tag{9.1}$$

where the right-hand side is the well-known *Lorentz force*. Equation 9.1 implies that

- the component of $\mathbf{k}$ parallel to $\mathbf{B}$ is constant;
- as $\frac{\mathrm{d}\mathbf{k}}{\mathrm{d}t}$ is perpendicular to $\mathbf{v}$ (defined property of the $\times$ operation) and as

$$\mathbf{v} = \frac{1}{\hbar}\nabla_{\mathbf{k}} E(\mathbf{k}) \tag{9.2}$$

(see Equation 5.5), $\frac{\mathrm{d}\mathbf{k}}{\mathrm{d}t}$ is perpendicular to $\nabla_{\mathbf{k}} E(\mathbf{k})$. This means that the electron path (orbit) is one of constant energy. To see this, consider $\frac{\mathrm{d}\mathbf{k}}{\mathrm{d}t}.\nabla_{\mathbf{k}} E(\mathbf{k}) = 0$ (because the two are perpendicular); writing this in components gives $\frac{\partial k_x}{\partial t}\frac{\partial E}{\partial k_x} + \frac{\partial k_y}{\partial t}\frac{\partial E}{\partial k_y} + \frac{\partial k_z}{\partial t}\frac{\partial E}{\partial k_z} \equiv \frac{\mathrm{d}E}{\mathrm{d}t}$ from the chain rule. Hence, $\frac{\mathrm{d}E}{\mathrm{d}t} = 0$.

In k-space, the possible electron orbits are therefore described by the intersections of surfaces of constant energy with planes perpendicular to $\mathbf{B}$.

9.2.2 The cyclotron frequency

Consider a section of k-space orbit of constant energy E in a plane perpendicular to $\mathbf{B}$ (see Figure 9.1). The time $t_2 - t_1$ taken to traverse the part of the orbit between $\mathbf{k}_1$ to $\mathbf{k}_2$ is

$$t_2 - t_1 = \int_{t_1}^{t_2} \mathrm{d}t = \int_{\mathbf{k}_1}^{\mathbf{k}_2} \frac{\mathrm{d}k}{|\dot{\mathbf{k}}|}, \tag{9.3}$$

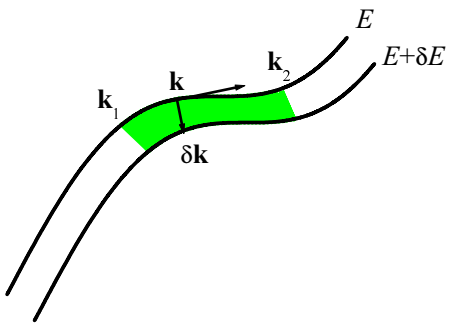

Figure 9.1: Geometrical interpretation of parameters used in the derivation of the cyclotron frequency; the two curves represent constant energy orbits of energy E and $E+\delta E$ in the plane perpendicular to the magnetic field. The electron traverses from $\mathbf{k}_1$ to $\mathbf{k}_2$ on the orbit of energy E; $\delta\mathbf{k}$ is perpendicular to the orbit of energy E and connects it to the orbit of energy $E+\delta E$. The small arrow perpendicular to $\delta\mathbf{k}$ shows the instantaneous direction of dk which runs along the orbit in the integral of Equation 9.4. The shaded area is the area of the k-space plane between orbits E and $E+\delta E$.

where $\dot{\mathbf{k}} = \frac{\mathrm{d}\mathbf{k}}{\mathrm{d}t}$. Equations 9.1 and 9.2 can be used to obtain $\dot{\mathbf{k}}$, so that Equation 9.3 becomes

$$t_2 - t_1 = \frac{\hbar^2}{eB}\int_{\mathbf{k}_1}^{\mathbf{k}_2} \frac{\mathrm{d}k}{|\nabla_{\mathbf{k}\perp} E|}, \tag{9.4}$$

where $\nabla_{\mathbf{k}\perp} E$ is the component of $\nabla_{\mathbf{k}} E$ perpendicular to the field.

The quantity $\nabla_{\mathbf{k}\perp}$ might seem rather nebulous;[1] however, it has a simple geometrical interpretation. Consider a second orbit in the same plane as the one of energy E defined at the start of this Section, but with energy $E+\delta E$ (see Figure 9.1). Let the vector $\delta\mathbf{k}$ join a point $\mathbf{k}$ on the orbit of energy E to a point on the orbit of energy $E+\delta E$, and let it also be perpendicular to the orbit of energy E at $\mathbf{k}$. If δE is small, then

$$\delta E = \nabla_{\mathbf{k}} E.\delta\mathbf{k} = \nabla_{\mathbf{k}\perp} E.\delta\mathbf{k}. \tag{9.5}$$

As $\nabla_{\mathbf{k}}$ is perpendicular to surfaces of constant energy, then $\nabla_{\mathbf{k}\perp}$ is perpendicular to the orbit of energy E and therefore parallel to $\delta\mathbf{k}$. Equation 9.5 becomes

$$\delta E = |\nabla_{\mathbf{k}\perp} E|\delta k, \tag{9.6}$$

so that Equation 9.4 can be rewritten

$$t_1 - t_2 = \frac{\hbar^2}{eB}\frac{1}{\delta E}\int_{\mathbf{k}_1}^{\mathbf{k}_2} \delta k \mathrm{d}k. \tag{9.7}$$

The integral in Equation 9.7 is the area of the k-space plane between orbits E and $E+\delta E$; therefore if $\delta E \to 0$ then

$$t_2 - t_1 = \frac{\hbar^2}{eB}\frac{\partial A_{1,2}}{\partial E}, \tag{9.8}$$

where $\frac{\partial A_{1,2}}{\partial E}$ is the rate at which the orbit from $\mathbf{k}_1$ to $\mathbf{k}_2$ sweeps ut area in k-space as E increases.

In most cases it is going to be useful to work in terms of closed orbits (cyclotron orbits) in k-space, *i.e.* closed paths where $\mathbf{k}_1 = \mathbf{k}_2$. In this case A becomes the area in k-space of the closed orbit; this will

[1] Or even "nablaous".

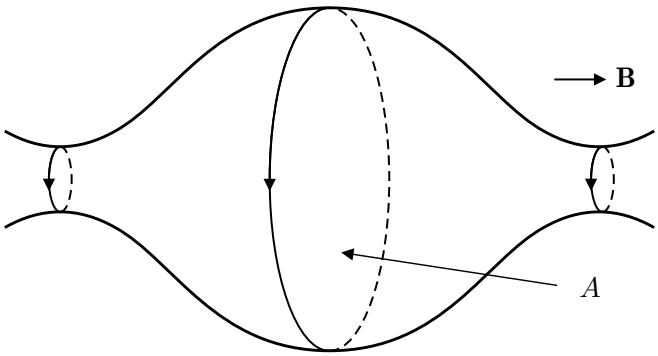

Figure 9.2: Orbits on a Fermi surface section are in planes perpendicular to **B**. Here, A represents the k-space cross-sectional area of the orbit.

depend on E and the component of **k** parallel to **B**, which we denote $k_{||}$. The period τ_c of the closed orbit is

$$\tau_c = \frac{\hbar^2}{eB}\frac{\partial A(E,k_{||})}{\partial E}; \tag{9.9}$$

turning this into an angular frequency ω_c (the *cyclotron frequency*), we obtain

$$\omega_c = \frac{eB}{m^*_{CR}}, \tag{9.10}$$

where

$$m^*_{CR} = \frac{\hbar^2}{2\pi}\frac{\partial A(E,k_{||})}{\partial E}. \tag{9.11}$$

The quantity m^*_{CR} defined in Equation 9.11 is known as the *cyclotron mass*. It is easy to show that for a free electron system this quantity is just m_e, so that Equation 9.10 yields the classical cyclotron frequency $\omega_c = eB/m_e$.[2]. Similarly, in the case of a constant, isotropic effective mass m^*, it can be shown in a straightforward manner that $\omega_c = eB/m^*$.

9.2.3 Orbits on a Fermi surface

Lectures 2–6 showed that the Fermi surface of a metal is a constant–energy surface *par excellence*. Therefore, if the material subjected to the magnetic field is metallic (*i.e.* possesses sections of Fermi surface), then Section 9.2.1 implies that the electrons will perform orbits in k-space about Fermi–surface cross–sections perpendicular to **B** (see Figure 9.2). Equations 9.10 and 9.11 can therefore give information about the cross-sectional areas of a section of Fermi surface. Note that the *sign* of $(\partial A/\partial E)$ allows the carriers on a section of Fermi surface to be identified as hole-like ($(\partial A/\partial E) < 0$) or electron-like ($(\partial A/\partial E) > 0$ in a very appealing manner (see Figure 9.3).

9.3 The introduction of quantum mechanics

9.3.1 Landau levels

A general proof of the quantised motion of a carrier in a magnetic field in an arbitrarily-shaped band is difficult. In this section, I shall use a band defined by the effective–mass tensor of problem set 2, with its minimum centred on $k = 0$ (a good approximation to many of the band extrema in semiconductors) and derive some analytical solutions for the eigenenergies of the electrons (the *Landau levels*). The anisotropic band also yields some useful insights about generalised bandstructure.

[2]See *e.g. Electricity and Magnetism*, by B.I. Bleaney and B. Bleaney, revised third/fourth editions (Oxford University Press, Oxford) page 126.

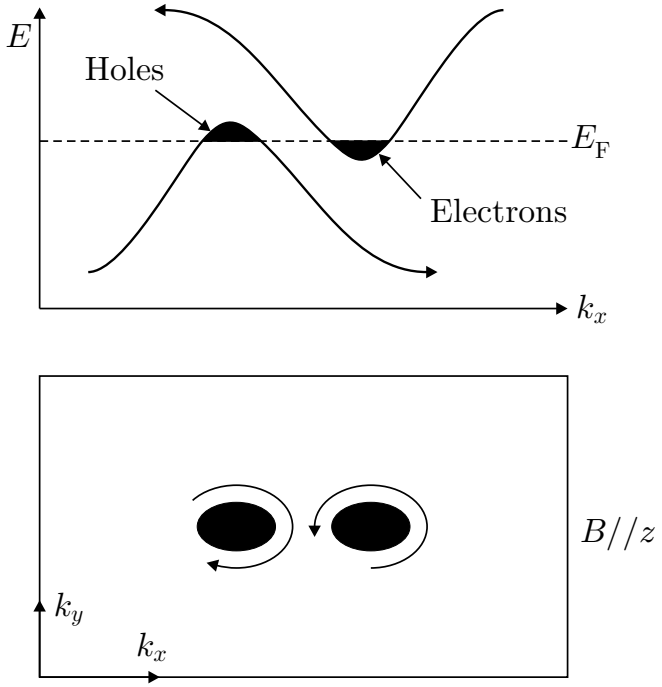

Figure 9.3: The use of the sign of $(\partial A/\partial E)$ to identify a section of Fermi surface as hole-like or electron-like. The top half of the Figure shows a schematic bandstructure with two bands crossing the Fermi energy E_F. E_F crosses the left-hand band near its maximum; the band is almost full, with holes (empty states) at the top of the band surrounded by filled states. E_F crosses the right-hand band near its minimum, so that there are electrons in the bottom of the band surrounded by empty states. The lower half of the Figure shows the corresponding Fermi-surface cross-sections. In the left-hand case, as E_F increases, the area of the section of Fermi surface decreases (hole-like). In the right-hand case, as E_F increases, the area of the section of Fermi surface increases (electron-like). The arrows show the opposite senses of cyclotron motion about the Fermi-surface sections.

For further generality, Section 9.3.2 will derive the Landau quantisation of arbitrarily-shaped bands in the limit that $\hbar\omega_c \ll E_F$.

The Hamiltonian for electrons in the band defined by the effective mass tensor of problem set 2, with its minimum centred on $k = 0$ is

$$\left\{ \frac{\mathcal{P}_x \mathbf{e}_1}{(2m_1)^{\frac{1}{2}}} + \frac{\mathcal{P}_y \mathbf{e}_2}{(2m_2)^{\frac{1}{2}}} + \frac{\mathcal{P}_z \mathbf{e}_3}{(2m_3)^{\frac{1}{2}}} \right\}^2 \psi = E\psi, \tag{9.12}$$

where the $\mathcal{P}$ are one-dimensional momentum operators; *i.e.* all of the effects of the crystalline potential have been absorbed into the bandstructure, which is defined by the effective masses. Substitution of a plane wave solution into Equation 9.12 yields energies of the correct form, *i.e.*

$$E = \frac{\hbar^2 k_x^2}{2m_1} + \frac{\hbar^2 k_y^2}{2m_2} + \frac{\hbar^2 k_z^2}{2m_3}. \tag{9.13}$$

Consider a magnetic field $\mathbf{B}$ directed along the z ($\mathbf{e}_3$) axis. In addition, remember that $\mathbf{B} = \nabla \times \mathbf{A}$, where $\mathbf{A}$ is the magnetic vector potential. One particular $\mathbf{A}$ which gives the correct $\mathbf{B}$ is

$$\mathbf{A} = (0, Bx, 0); \tag{9.14}$$

this choice is known as the *Landau gauge*. For an electron in a magnetic field,

$$\mathcal{P} \rightarrow (\mathcal{P} + e\mathbf{A}). \tag{9.15}$$

Making such a substitution into Equation 9.12 gives

$$\left\{ \frac{\mathcal{P}_x \mathbf{e}_1}{(2m_1)^{\frac{1}{2}}} + \frac{(\mathcal{P}_y + eBx)\mathbf{e}_2}{(2m_2)^{\frac{1}{2}}} + \frac{\mathcal{P}_z \mathbf{e}_3}{(2m_3)^{\frac{1}{2}}} \right\}^2 \psi = E\psi. \tag{9.16}$$

All that we have done is introduce an extra term with x in it; as $[\mathcal{P}_y, x] = [\mathcal{P}_z, x] = 0$.[3] $\mathcal{P}_y$ and $\mathcal{P}_z$ still commute with the Hamiltonian; their associated physical quantities are thus constants of the motion. The operators $\mathcal{P}_y$ and $\mathcal{P}_z$ in Equation 9.16 can therefore be replaced by their constant values $\hbar k_y$ and $\hbar k_z$ respectively. Equation 9.16 becomes

$$\left\{ \frac{\mathcal{P}_x \mathbf{e}_1}{(2m_1)^{\frac{1}{2}}} + \frac{(\hbar k_y + eBx)\mathbf{e}_2}{(2m_2)^{\frac{1}{2}}} + \frac{\hbar k_z \mathbf{e}_3}{(2m_3)^{\frac{1}{2}}} \right\}^2 \psi = E\psi. \tag{9.17}$$

Squaring the bracket, remembering that the Cartesian unit vectors $\mathbf{e}_j$ are mutually perpendicular (*i.e.* $\mathbf{e}_j.\mathbf{e}_l = \delta_{j,l}$), gives

$$\left\{ \frac{\mathcal{P}_x^2}{2m_1} + \frac{(\hbar k_y + eBx)^2}{2m_2} + \frac{\hbar^2 k_z^2}{2m_3} \right\} \psi = E\psi. \tag{9.18}$$

Making the substitutions $E' = E - (\hbar^2 k_z^2/2m_3)$ and $x_0 = -(\hbar k_y/eB)$, and rearranging yields

$$\{ \frac{\mathcal{P}_x^2}{2m_1} + \frac{e^2 B^2}{2m_2}(x - x_0)^2 \} \psi = E'\psi. \tag{9.19}$$

Equation 9.19 looks exactly like the Hamiltonian of a one-dimensional harmonic oscillator, *i.e.*,

$$\{ \frac{\mathcal{P}_x^2}{2m} + \frac{1}{2} m\omega^2 (x - x_0)^2 \} \psi = E'\psi, \tag{9.20}$$

with $\omega = eB/(m_1 m_2)^{\frac{1}{2}}$; thus $E' = (l + \frac{1}{2})\hbar\omega$, with $l = 0, 1, 2, 3.....$ The energy levels of the electron are therefore

$$E(l, B, k_z) = \frac{\hbar^2 k_z^2}{2m_3} + (l + \frac{1}{2})\hbar\omega, \tag{9.21}$$

[3] These are standard commutation relationships; see *e.g.* *Quantum Mechanics*, by Stephen Gasiorowicz (Wiley, New York 1974) pages 51, 141.

with

$$\omega = eB/(m_1 m_2)^{\frac{1}{2}} \equiv \omega_c. \tag{9.22}$$

The equivalence of ω and ω_c, the cyclotron frequency for this geometry (*i.e.* $\omega_c = eB/m^*_{\rm CR}$, with $m^*_{\rm CR} = \frac{\hbar^2}{2\pi}\frac{\partial A(E,k_{||})}{\partial E}$), is left to the reader.

The following points may be deduced from Equation 9.21.

- The energy of the electron's motion in the plane perpendicular to **B** is completely quantised. These quantised levels are known as *Landau levels*.
- The k-space areas of the orbits in the plane perpendicular to **B** are also quantised (this is easy to work out in the present case and is left as an exercise); thus, allowed orbits fall on "Landau tubes" in k-space with quantised cross-sectional area.
- The energy "quantum" for the in-plane motion appears to be $\hbar\times$(the semiclassical cyclotron frequency).
- The motion parallel to **B** is unaffected (*c.f.* Section 9.2.1).

We shall consider the second point in more detail (and more generally) in the following section.

9.3.2 Application of Bohr's correspondence principle to arbitrarily-shaped Fermi surfaces in a magnetic field

In Section 9.4 below we are going to consider the effect of the quantisation of the k-space orbits caused by **B** on the Fermi surfaces of metals; *i.e.* we shall be dealing with Landau levels which cut the Fermi surface. The Fermi surfaces of real metals are in general not as simple as the case dealt with in the previous section. Therefore, in order to treat an arbitrily-shaped band, resulting in an arbitrarily-shaped Fermi surface, we shall use Bohr's correspondence principle, which states in this context that the difference in energy of two adjacent levels is $\hbar$ times the angular frequency of classical motion at the energy of the levels.

The correspondence principle is only valid for levels with very large quantum numbers. However, this is not really a problem, as we are going to be dealing with Landau levels with energies comparable to $E_{\rm F}$; in most metals $E_{\rm F}$ is ∼several eV, whereas the cyclotron energy of free electrons is $\hbar eB/m_{\rm e} \approx 1.16\times10^{-4}$ eV at $B = 1$ T. Laboratory fields are usually ~ 10 T, and so the quantum numbers of Landau levels with energies $\sim E_{\rm F}$ will be $l \sim 10^4$; the correspondence principle should work reasonably well.

The classical frequency at the energy of interest (*i.e.* $E_{\rm F}$) is given by Equation 9.10

$$\omega_c = \frac{eB}{m^*_{\rm CR}}, \tag{9.23}$$

with $m^*_{\rm CR}$ given by Equation 9.11 as follows

$$m^*_{\rm CR} = \frac{\hbar^2}{2\pi}\frac{\partial A(E,k_{||})}{\partial E}. \tag{9.24}$$

Here, A is now specifically *the cross-sectional area of the Fermi surface in a plane perpendicular to* **B**. Thus, the separation in energy of two Landau tubes with energies close to $E_{\rm F}$ is

$$E(l+1,B,k_{||}) - E(l,B,k_{||}) = \frac{\hbar eB}{m^*_{\rm CR}}, \tag{9.25}$$

with $m^*_{\rm CR}$ defined by Equation 9.24. (It is interesting to compare this Equation with Equation 9.21.)

9.3.3 Quantisation of the orbit area

Equation 9.25 may be rewritten as

$$(E(l+1,B,k_{||})-E(l,B,k_{||}))\frac{\partial A(E)}{\partial E}=\frac{2\pi eB}{\hbar}. \tag{9.26}$$

Now as the E in $A(E)$ is of order E_{F}, then the difference between adjacent levels will be $\ll$ the energies of the levels themselves. Thus the approximation

$$\frac{\partial A(E)}{\partial E}=\frac{A(E(l+1,B,k_{||}))-A(E(l,B,k_{||}))}{E(l+1,B,k_{||})-E(l,B,k_{||})} \tag{9.27}$$

may be made, so that Equation 9.26 becomes

$$A(E(l+1,B,k_{||}))-A(E(l,B,k_{||}))=\frac{2\pi eB}{\hbar}. \tag{9.28}$$

This states that classical orbits at adjacent allowed energies and the same $k_{||}$ enclose k-space areas that differ by a fixed amount δA, with

$$\delta A=\frac{2\pi eB}{\hbar}. \tag{9.29}$$

Putting this another way, the k-space area enclosed by an orbit of allowed energy and $k_{||}$ must be given by

$$A(E(l+1,B,k_{||}))=(l+\lambda)\delta A=(l+\lambda)\frac{2\pi eB}{\hbar} \tag{9.30}$$

for large l, where λ is a constant ~ 1.

As in Section 9.3.1, we have found "Landau tubes" which define the allowed k-space orbits; rather than being quasicontinuous, the Fermi surface will now be composed of occupied states lying on Landau tubes (see Figure 9.4. Note that the k-space area of each tube increases with B; as we shall see in the sections below, this means that tubes "pop out" of the Fermi surface as B increases.

9.3.4 The electronic density of states in a magnetic field

The above sections have shown that the energy of the band electron is completely quantised into Landau levels in the plane perpendicular to $\mathbf{B}$, whilst the motion parallel to $\mathbf{B}$ remains unconstrained. This means that the density of states of the electrons is an infinite "ladder" of Landau levels, each with a one-dimensional density of states function, due to the motion parallel to $\mathbf{B}$, superimposed.[4] The overall density of states will therefore be of the form $g(E)=\sum_{l=0}^{\infty}C(E-E(l,B))^{-\frac{1}{2}}$, where $E(l,B)$ is the energy of the Landau level (*i.e.* the lowest energy point on the Landau tube) and C is a constant; it is shown schematically in Figure 9.5.

9.4 Quantum oscillatory phenomena

Each time one of the sharp peaks in the electronic density of states moves through the chemical potential μ,[5] there will be a modulation of the density of states at μ. Since almost all of a metal's properties depend on the density of states at μ, we expect this to affect the behaviour of the metal in some way.

Figure 9.6 shows a Landau tube superimposed on constant energy surfaces E and $E+\delta E$. The left-hand part of the figure shows the general case; as the field increases, the tube sweeps outwards, so that some of its states are always crossing the constant energy surfaces. However, in the right-hand part of the figure, the tube reaches an *extremal cross-section* of the constant energy surface E. In this case,

[4] In other words, as far as the density of states is concerned, the magnetic field reduces the effective dimensionality of the electron system by 2.

[5] Remember from earlier lectures that $E_{\mathrm{F}}\equiv\mu(T=0)$. In many books, quantum oscillations are said to result from "Landau levels passing through the Fermi energy". This is only strictly true at $T=0$; the chemical potential is the important energy as far as the electrons are concerned. In metals at low temperatures there will be a very small difference between E_{F} and μ; nevertheless, one should not tolerate sloppy terminology.

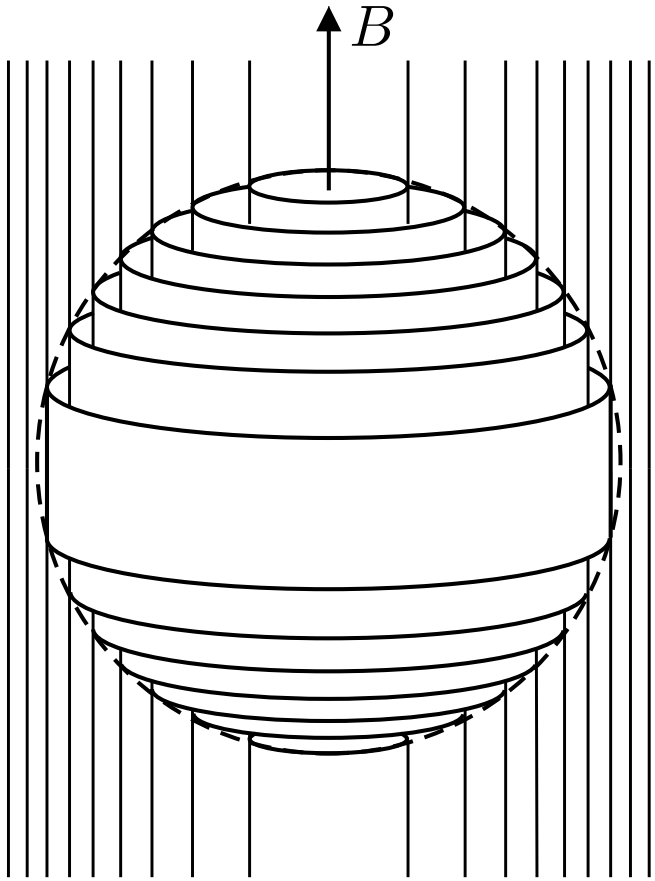

Figure 9.4: Schematic of a Fermi sphere rearranged into Landau tubes.

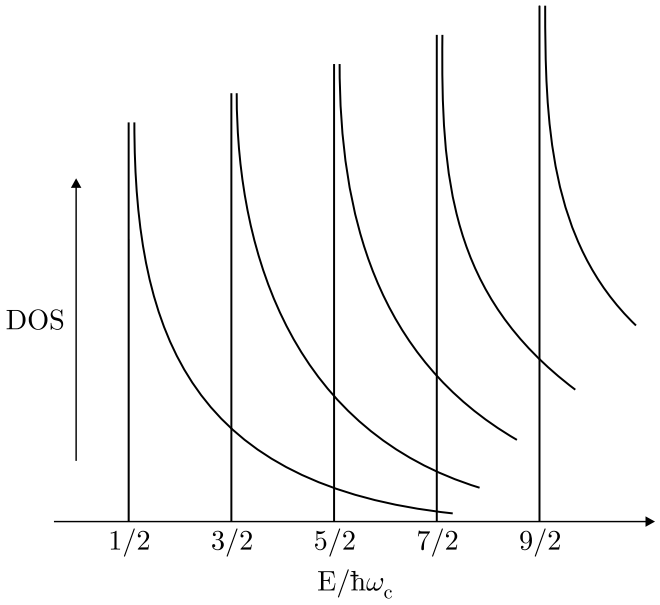

Figure 9.5: Schematic of the electronic density of states in a magnetic field. The "sawtooth" structure results from a one-dimensional density of states (from the motion parallel to **B**) superimposed on the δ-function-like Landau levels.

a much larger area of the cylinder (and therefore a much greater number of states, which lie uniformly in k-space) lies between E and $E+\delta E$. Returning to the case of the Fermi surface, we can therefore say that the maximum effect of the Landau quantisation will occur when a Landau tube (and its associated peak in the density of states) crosses an extremal cross-section of a Fermi surface. By analogy with the discussion of classical orbits about the Fermi surface in Section 9.2.1, such cross-sections are often known as *extremal orbits*.

The Landau tube crosses an extremal orbit/cross-section when

$$(l+\lambda)\frac{2\pi eB}{\hbar} = A_{\text{ext}}, \tag{9.31}$$

where A_{ext} is the k-space area of the extremal cross-section of the Fermi surface in a plane perpendicular to $\mathbf{B}$. Thus, the metal's properties will oscillate as $\mathbf{B}$ changes, with a period given by

$$\Delta\left(\frac{1}{B}\right) = \frac{2\pi e}{\hbar}\frac{1}{A_{\text{ext}}}. \tag{9.32}$$

Such oscillations are known generically as *magnetic quantum oscillations*.

Often it is more convenient to describe a series of quantum oscillations using a frequency known as the *fundamental field*

$$B_{\text{F}} = \frac{1}{\Delta(1/B)} = \frac{\hbar}{2\pi e}A_{\text{ext}}. \tag{9.33}$$

Note that

- the fundamental field of the quantum oscillations is determined solely by the Fermi surface extremal area and fundamental constants;
- several different frequencies (fundamental fields) of quantum oscillation may be simultaneously present for a given orientation of $\mathbf{B}$, corresponding to different possible extremal orbits (see Figure 9.7); a famous example is the simultaneous observation of frequencies from "neck and belly" orbits in Cu and Au;
- a measurement of the observed frequencies as a function of magnetic field orientation allows the Fermi-surface shape to be mapped out;
- open orbits do not give rise to quantum oscillations.[6]

9.4.1 Types of quantum oscillation

As the electronic density of states at E_{F} determines most of a metal's properties, virtually all properties will exhibit quantum oscillations in a magnetic field. Examples include[7]

- oscillations of the magnetisation (the de Haas–van Alphen effect);
- oscillations of the magnetoresistance (the Shubnikov–de Haas effect);
- oscillations of the sample length;
- ocillations of the sample temperature;
- oscillations in the ultrasonic attenuation;
- oscillations in the Peltier effect and thermoelectric voltage;
- oscillations in the thermal conductivity.

[6] However, open orbits do lead to a very interesting quantum phenomenon which has recently been observed in high-frequency experiments; see A. Ardavan *et al., Phys. Rev. B* **60**, 15500 (1999); *Phys. Rev. Lett.* **81**, 713 (1998).

[7] Some pictures of typical data are shown in *Solid State Physics*, by N.W Ashcroft and N.D. Mermin (Holt, Rinehart and Winston, New York 1976) pages 266-268.

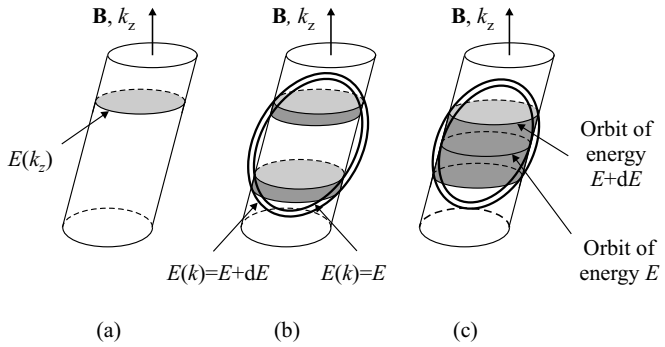

Figure 9.6: Schematic of Landau tubes crossing surfaces of constant energy E and $E + \delta E$. (a) shows the Landau tube on its own; (b) shows the Landau tube intersecting constant energy surfaces E and $E+\delta E$ when the tube does not correspond to an extremal orbit; (c) shows the Landau tube intersecting constant energy surfaces E and $E+\delta E$ when the tube corresponds to an extremal orbit. In (c), a much greater area of the cylinder (and therefore a larger number of states) lies between E and $E + \delta E$ than is the case in (b).

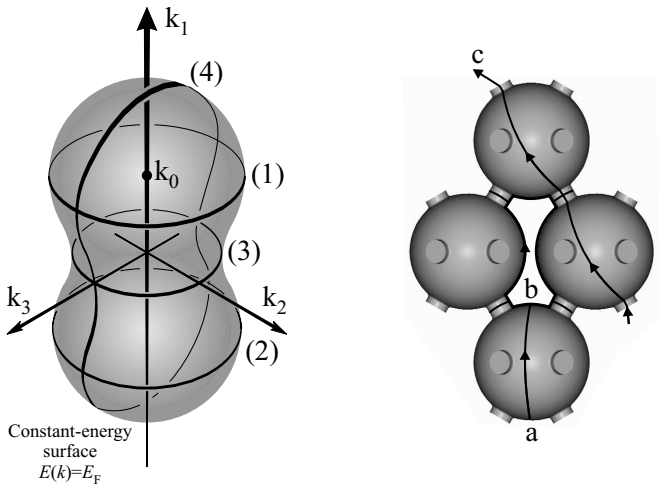

Figure 9.7: Illustration of the types of extremal orbit about Fermi surfaces which can give rise to quantum oscillations. The left-hand figure shows that for **B** parallel to k_1 there will be three extremal orbits ((1), (2) and (3)); as (1) and (2) have the same area, there will be two series of quantum oscillation (*i.e.* two different frequencies will be present). However, for **B** parallel to k_2, there is only one extremal orbit (4); a similar situation would apply if **B** were parallel to k_3. The right-hand figure helps to visualise the different types of orbit possible in metals possessing necks and bellies in their Fermi surfaces, such as Copper, Silver or Gold. The orbit labelled a is an orbit around the "belly" of the Fermi surface. If the magnetic field is applied out of the page, then an extremal "hole-like" orbit (labelled b) will occur around the bone-shaped space in the middle; this is known as the *dog's bone* orbit! In orbit c, electrons run across the bellies and necks in an extended or *open* orbit; *this does not give rise to quantum oscillations*, as there is no closed orbit with which a frequency can be associated. If the magnetic field is applied along one of the neck directions, extremal orbits about both neck and belly are possible, leading to two frequencies of quantum oscillations. Note that different field orientations are required to observe the different cases; the orbits in k-space are *always* in planes perpendicular to **B**.

9.4.2 The de Haas–van Alphen effect

The de Haas-van Alphen effect is perhaps the most significant of the quantum oscillatory phenomena in metals; as the magnetisation M is a thermodynamic function of state;[8] it can be directly related to the density of states and Fermi–Dirac distribution function of the electrons in a metal, *without additional assumptions*. This means that theoretical models for the Fermi surface can be checked in a very rigorous manner.[9]

Figure 9.8 shows a schematic of the types of coil most commonly used to observe the de Haas–van Alphen effect. Each system consists of a coil c which contains the sample and a *compensating coil* c^0; both are placed in a time-varying magnetic field. The coils c and c^0 are connected in series-opposition and carefully balanced so that in the absence of a sample the voltage induced by $\mathrm{d}B/\mathrm{d}t$ in c^0 exactly cancels that in c. When the sample is placed in c, then c and c^0 are no longer balanced; a voltage V is induced, where

$$V = \alpha \frac{\mathrm{d}M}{\mathrm{d}B}\frac{\mathrm{d}B}{\mathrm{d}t}. \tag{9.34}$$

Here α is a parameter depending on the geometry of the coil and sample. The de Haas–van Alphen oscillations occur in $\mathrm{d}M/\mathrm{d}B$ and thus will be visible in V.[10]

The field is provided in two ways.

- For fields of up to $\sim$ 20 T, superconducting magnets are generally used. The magnet consists of two parts, a large outer coil providing a static field and an inner coil which provides a small modulation field (*i.e.* $\mathrm{d}B/\mathrm{d}t$) of mT amplitude at a few tens of Hz.
- Pulsed magnets are used for fields of up to $\sim$ 60 T; in this case the magnetic field rises to its maximum value in a few ms, so that $\mathrm{d}B/\mathrm{d}t$ is large (there is no need for an additional modulation coil).

Some typical de Haas-van Alphen data are shown in Figures 9.9 and 9.10.

The coils are often mounted on a rotation stage so that the sample can be rotated *in situ*, allowing measurements to be made with **B** applied at several orientations to the crystal axes. The coils and sample are mostly mounted in ^{3}He cryostats or dilution refrigerators, as mK temperatures are needed to observe the oscillations in many cases (see below).

9.4.3 Other parameters which can be deduced from quantum oscillations

So far we have concentrated on the information about the Fermi-surface shape provided by the quantum oscillations. However, other valuable information can be deduced. Figure 9.11 shows Shubnikov–de Haas oscillations in an organic solid (see Section 8 for more details of this sort of conductor). Two things are immediately obvious.

1. **The oscillations grow in amplitude as the temperature is lowered.** This occurs because finite temperatures "smear out" the edge of the Fermi-Dirac distribution function which separates filled and empty states (see Figure 1.7). At $T = 0$ the Landau tubes will pop out of a very sharp Fermi surface; at finite T the surface will be "fuzzy". The modulation of the density of states around μ caused by the Landau tubes will therefore be less significant. The thermal smearing implies that $\hbar\omega_\mathrm{c}$ must be greater than $\sim k_\mathrm{B}T$ for oscillations to be observed, *i.e.* low temperatures are needed.

   As the decline in intensity is caused by the Fermi-Dirac distribution function, it can be modelled rather well, and an analytical expression for the temperature dependence of the oscillation amplitude, valid as long as the oscillation amplitude is small, has been derived[11]

$$\text{Amplitude} \propto \frac{\chi}{\sinh\chi}, \tag{9.35}$$

[8] See *e.g. Equilibrium Thermodynamics* by C.J Adkins, Third Edition (Cambridge University Press, Cambridge 1983) page 6 and Appendix.

[9] For enthusiasts, a relatively recent example of this is given in *A numerical model of quantum oscillations in quasi-two-dimensional organic metals in high magnetic fields*, by N. Harrison *et al.*, *Physical Review B*, **54**, 9977 (1996).

[10] de Haas-van Alphen oscillations are also sometimes observed using a *torque magnetometer*; see J.S. Brooks *et al.*, *Rev. Sci. Instrum.* **64**, 3248 (1987).

[11] See *Magnetic oscillations in metals*, by David Shoenberg (Cambridge University Press, Cambridge 1984) Chapter 2.

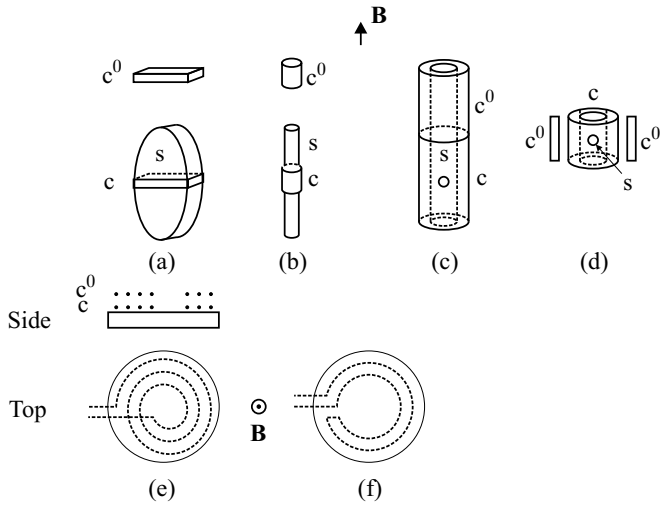

Figure 9.8: Coils for the observation of the de Haas–van Alphen effect. For each set, c is the coil flux-linked to the sample and c^0 is the compensating coil, only weakly flux-linked to the sample: (a) c is wound around the centre of a disc-like sample; (b) c is wound around a sample cut into a cylinder; (c) a small sample inside colinear coils c and c^0; (d) small sample inside coaxial coils c and c^0; (e) side and top views of a coil evaporated down onto a thin sample; (f) as (e) but with only a single annular turn. In both (e) and (f) c^0 has not been shown. (Based on figures in *Magnetic oscillations in metals*, by David Shoenberg (Cambridge University Press, Cambridge 1984).)

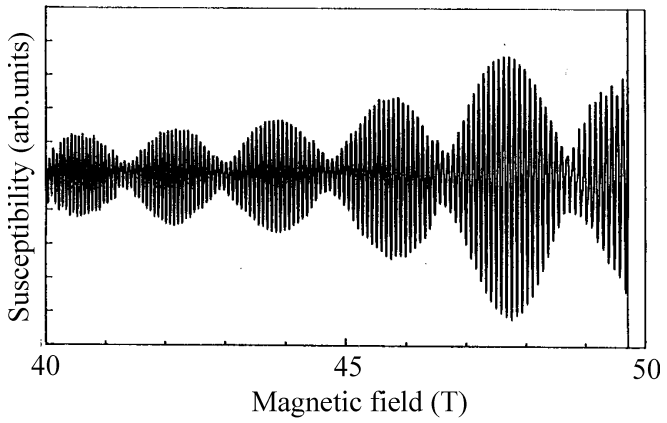

Figure 9.9: de Haas-van Alphen oscillations in Pt at 4.2 K with **B** parallel to [111]. The data have been recorded using a pulsed magnetic field. Note the presence of two frequencies of oscillations due to two extremal orbits about the Fermi surface. The y axis, labelled "susceptibility", represents the voltage V induced in the coil divided by $(\mathrm{d}B/\mathrm{d}t)$, leaving a quantity proportional to the differential susceptibility $(\mathrm{d}M/\mathrm{d}B)$ (see Equation 9.34). (Data from S. Askenazy, Physica B **201**, 26 (1994).)

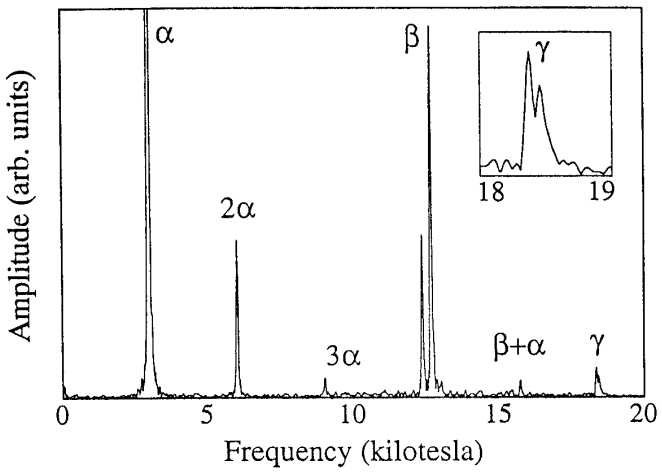

Figure 9.10: Fourier transform of de Haas-van Alphen oscillations of Sr_2RuO_4. Fourier transformation is routinely used to help understand de Haas-van Alphen oscillations. The oscillation data (recorded digitally) are processed so that they are equally spaced in $1/B$; the resulting file is Fourier transformed using a desk-top computer. Each extremal cross-section of the Fermi-surface generates a peak in the Fourier transform, the frequency of which is proportional to the k-space area. Oscillations which are non-sinusoidal in shape generate harmonics in the Fourier transform; frequency mixing effects also occur, resulting in sum frequencies. Three Fermi-surface cross-sections (labelled α, β and γ) are shown, along with some harmonics of α and a sum frequency $\beta+\alpha$. (Data from A.P. McKenzie *et al.*, *J. Phys. Soc. Jpn.* **67**, 385 (1998)).

where $\chi = 14.7 m^*_{\rm CR} T/B$ (with T in Kelvin and B in Tesla) . It is fairly obvious that the parameter χ is proportional to the ratio $k_{\rm B}T/\hbar\omega_{\rm c}$; *i.e.* what we are doing is comparing $k_{\rm B}T$ and $\hbar\omega_{\rm c}$. Fits of the oscillation amplitude to Equation 9.35 can therefore be used to give $m^*_{\rm CR}$.

2. **The oscillations grow in amplitude as B increases.** This occurs because scattering causes the Landau levels to have a finite energy width $\sim \hbar/\tau$. As B increases, $\hbar\omega_{\rm c}$ will increase, so that the broadened Landau levels will become better resolved; theoretical studies have shown that this causes the oscillation amplitude to vary with B as follows (again, the equation is only valid for small oscillations)

$$\text{Amplitude} \;\propto\; e^{-\frac{\pi}{\omega_{\rm c}\tau}}. \tag{9.36}$$

Therefore the scattering rate τ^{-1} can be extracted.

In addition, information about the g-factor of the electrons can be obtained from the oscillations under certain circumstances.[12]

9.4.4 Magnetic breakdown

The frequencies observed in the quantum oscillations correspond to the areas of closed semiclassical orbits about the extremal areas of the Fermi surface. However, under certain circumstances, much higher frequency oscillations can become apparent at high fields, corresponding to larger k-space areas. These are caused by *magnetic breakdown*.

Figure 9.12 shows a simple Fermi surface cross-section with two open semiclassical orbits (incapable of giving quantum oscillations) and a closed orbit (capable of giving quantum oscillations); the arrows show the electron trajectories. At low fields, one frequency of oscillations corresponding to the closed orbit will be seen. At high fields, the electrons have sufficient cyclotron energy to tunnel *in k-space* from one part of the Fermi surface to another. Therefore they can now describe much larger closed k-space

[12]See *Magnetic oscillations in metals*, by David Shoenberg (Cambridge University Press, Cambridge 1984) and J. Singleton, *Reports on Progress in Physics*, **63**, 1111 (2000).

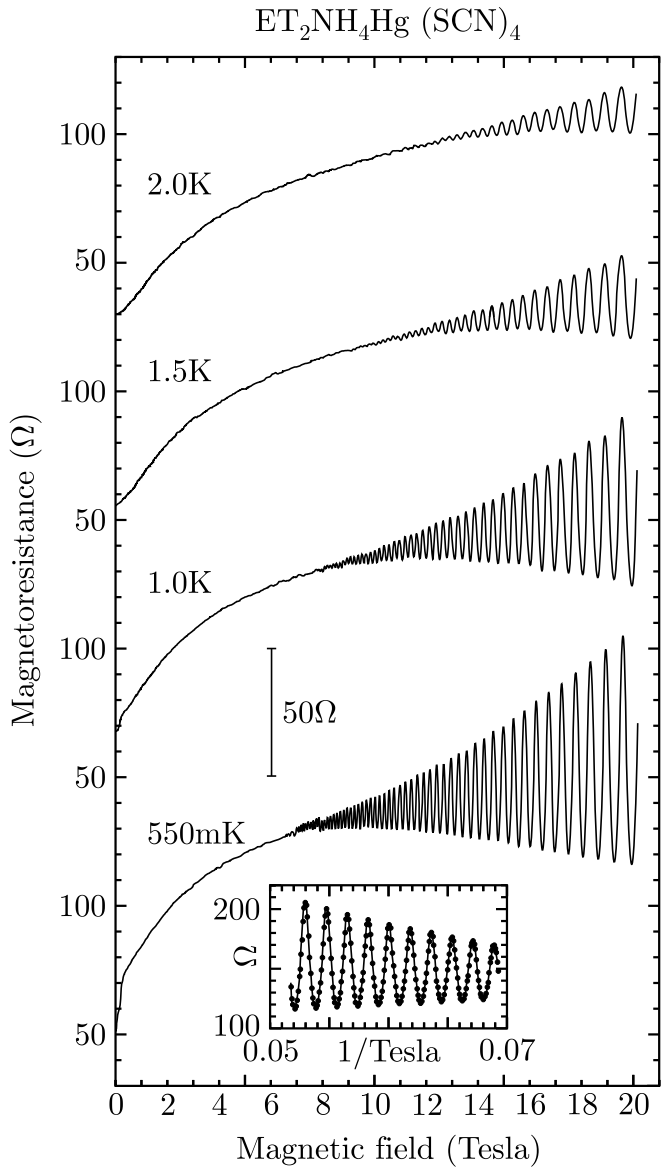

Figure 9.11: Shubnikov–de Haas oscillations in the organic molecular solid α-(BEDT-TTF)$_2$NH$_4$Hg(SCN)$_4$; data for different temperatures have been offset for clarity. The inset shows that the oscillations are periodic in $1/B$. (Data from J. Singleton, *Reports on Progress in Physics*, **63**, 1111 (2000).)

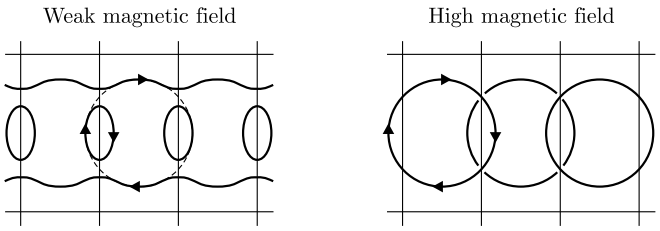

Figure 9.12: Explanation of magnetic breakdown. Left: semiclassical orbits on a simple Fermi surface at low fields; right: magnetic breakdown at high fields.

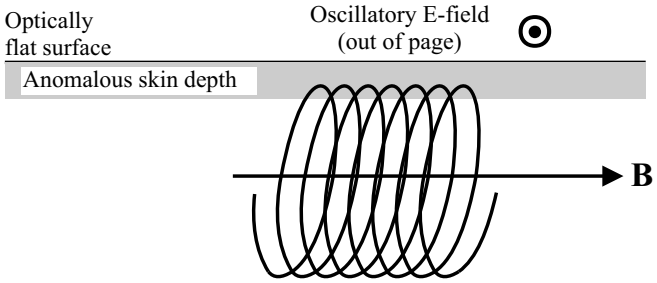

Figure 9.13: Geometry of a cyclotron resonance experiment in a metal. The shaded region indicates the skin depth for the radiation; the helical orbits of the electrons are shown schematically.

orbits, leading to higher-frequency quantum oscillations. In effect, the magnetic field is beginning to break down the arrangement of the bandstructure at zero field.

We shall see an example of magnetic breakdown later.

9.5 Cyclotron resonance

It is possible to make a direct measurement of ω_c using millimetre-waves or far-infrared radiation to excite transitions between Landau levels. Such an experiment is known as *cyclotron resonance*. The conditions for observing cyclotron resonance in metals and semiconductors are rather different, and the two cases are described below.

9.5.1 Cyclotron resonance in metals

The field components of electromagnetic radiation decay with distance z into a conducting material as $\exp(-z/\delta)$, where $\delta = (\frac{1}{2}\sigma\omega\mu_r\mu_0)^{-\frac{1}{2}}$ is the *skin depth* or anomalous skin depth; here σ is the conductivity of the material, $\mu_r\mu_0$ is its permeability and ω is the angular frequency of the radiation. Metals have rather high conductivities and hence small skin depths; typical values for Copper are $\delta \approx 7\times10^{-5}$m at $\omega/2\pi \approx 1$ MHz and $\delta \approx 7\times10^{-7}$m at $\omega/2\pi \approx 10$ GHz. [13] Typical effective masses in metals combined with the magnetic fields readily available in laboratories have meant that frequencies $\omega/2\pi \sim 1-100$ GHz have tended to be applied in cyclotron resonance experiments (see *Band theory and electronic properties of solids*, by John Singleton (Oxford University Press, 2001) Chapter 8). At such frequencies, radiation cannot penetrate far into the crystal, dictating the geometry of the cyclotron resonance measurement (see Figure 9.13). The magnetic field is applied parallel to a surface of the crystal, which is placed in a region of oscillating electric field in a resonant cavity; **E** of the radiation is arranged to be perpendicular to **B** and parallel to the surface. If the frequency of the radiation $\omega = j\omega_c$, where j is an integer, then the electrons will receive a "kick" from the radiation's electric field every

[13] The skin depth is derived in *Electricity and Magnetism*, by B.I. Bleaney and B. Bleaney, revised third/fourth editions (Oxford University Press, Oxford) page 236.

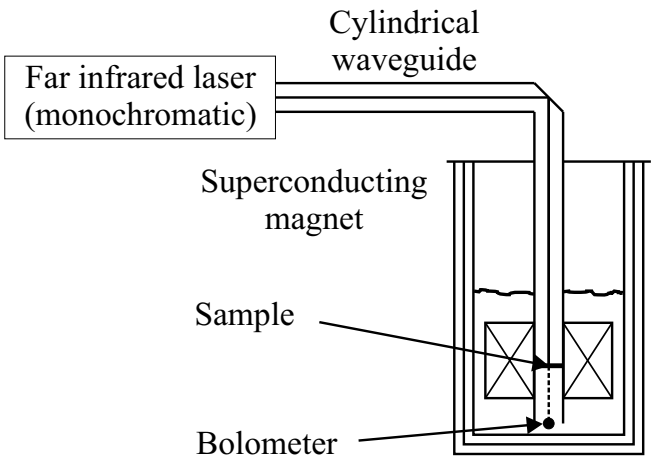

Figure 9.14: Schematic of a cyclotron resonance experiment in a semiconductor.

time they come within a skin depth of the surface; this results in absorption of energy. Usually ω is kept constant and the field is swept, so that absorptions are uniformly spaced in $1/B$. As in the case of the quantum oscillations, low temperatures are required. A magnetic field which is very accurately parallel to the sample's surface is required for a successful measurement. This type of experiment is often referred to as *the Azbel'–Kaner geometry.*

9.5.2 Cyclotron resonance in semiconductors

The number densities of carriers in semiconductor samples are much lower than those in metals, so that the radiation can completely penetrate even large samples. A simple transmission arrangement is usually adopted (see Figure 9.14). The cyclotron resonance is usually recorded by measuring the sample transmission; experiments are carried out either by fixing the magnetic field and varying the energy of the radiation (see Figure 9.15), or by using a fixed-frequency source (such as a far-infrared laser, which can give a number of monchromatic laser lines in the wavelength range 40 μm to 1000 μm) and sweeping the magnetic field (see Figures 9.14 and 9.16).[14] The magnetic field is usually provided by a superconducting magnet ($B = 0- \sim 20$ T). As the whole of the cyclotron orbit experiences the electric field of the radiation (*c.f.* the situation in metals; see above), the quantum-mechanical selection rule for the Landau-level quantum number ($\Delta l = \pm 1$) holds. Thus the resonance condition is

$$\omega = \omega_{\rm c} = \frac{eB}{m^*_{\rm CR}}, \tag{9.37}$$

where ω is the angular frequency of the radiation.

The linewidth of the resonance can give information about the scattering rate τ^{-1}. The scattering induces a frequency uncertainty $\Delta\omega_{\rm c} \sim \tau^{-1}$. If the experiment is a fixed-frequency, swept-field one, this translates to an uncertainty (*i.e.* resonance width) in magnetic field of $\Delta B = \Delta\omega_{\rm c} m^*_{\rm CR}/e \sim m^*_{\rm CR}/e\tau$.[15]

In the case of degenerate semiconductor systems (*e.g.* heterojunctions), free carriers are present even at low temperatures; typical cyclotron resonance data are shown in Figure 9.15. However, in lightly doped samples, the carriers must be excited into the bands by either raising the temperature to cause the impurities to ionise (but not so far as to broaden the Landau levels) or by additionally illuminating the sample with above-band-gap radiation.

[14] An alternative arrangement for semiconductor cyclotron resonance (rather an old-fashioned one) is given in *Electricity and Magnetism*, by B.I. Bleaney and B. Bleaney, revised third/fourth editions (Oxford University Press, Oxford) pages 729-734; the description also provides a more rigorous derivation of the linewidth of the cyclotron resonance than the one given here.

[15] Provided that $m^*_{\rm CR} \approx m^*$, the carrier effective mass for linear motion (and this is often true in direct-gap semiconductors like GaAs) it is apparent that $1/\Delta B \sim$ the carrier mobility.

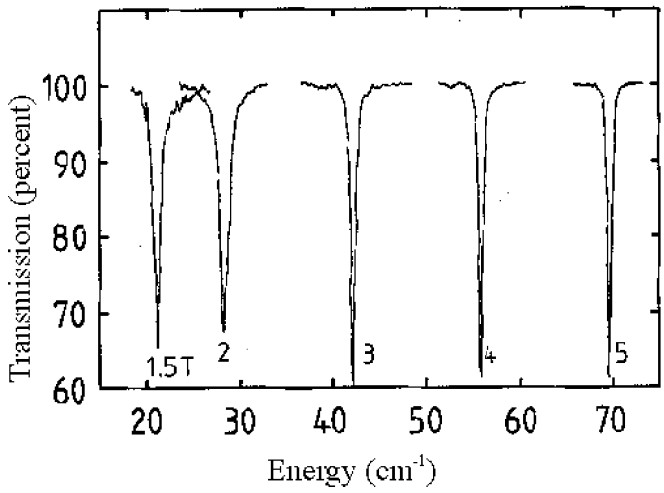

Figure 9.15: Cyclotron resonances in a GaAs-(Ga,Al)As heterojunction at $T = 4.2$ K; the magnetic field has been applied perpendicular to the two-dimensional electron layer, which has an areal carrier density of $\sim 9 \times 10^{10}\text{cm}^{-2}$. The data have been recorded by fixing the magnetic field at 1.5, 2, 3, 4, and 5 T; at each field, a Fourier-transform spectrometer has then been used to record the transmission of the sample as a function of energy. (Data recorded by G. Wiggins, University of Oxford. For further data of this type, see C.J.G.M. Langerak *et al., Phys. Rev. B.* **38** 13133 (1988).)

Material	$m_1 = m_2$	m_3	m_{lCR}	m^*_{hCR}
Ge	0.082	1.64	0.044	0.3
Si	0.19	0.98	0.16	0.3

Table 9.1: Effective masses (in units m_e) in Ge and Si determined using cyclotron resonance. The masses m_1, m_2 and m_3 refer to the components of the effective mass tensors for the conduction band; m_{lCR} and m^*_{hCR} are the cyclotron masses of light and heavy holes respectively.

Figure 9.16 shows an example of the latter technique applied to a single crystal of Ge. In addition to separate resonances caused by light and heavy holes, three electron cyclotron resonances are observed. This occurs becaue the anisotropic conduction-band minima in Ge lie along the [111] axes (see Figure 6.6); in Figure 9.16 the static magnetic field makes three different angles with the four [111] axes. The conduction-band minima in Ge can be described using an effective mass tensor; if one of the principal axes of the co-ordinate system is directed along a [111] axis, then the tensor is diagonal. Under such circumstances (see second problem set), the cyclotron resonance occurs at $\omega = \frac{eB}{m^*}$, with

$$m^* = \left(\frac{B^2 m_1 m_2 m_3}{m_1 B_x^2 + m_2 B_y^2 + m_3 B_z^2} \right)^{\frac{1}{2}},$$

where the components of the magentic field (B_1, B_2, B_3) are defined with respect to the principal axes which make the tensor diagonal. Thus, the cyclotron resonance frequency depends on the orientation of the static magnetic field with respect to the crystal axes. Such angle-dependent cyclotron resonance experiments can be used to determine components of the effective mass tensor.

In the case of Ge and Si, it is found that two of the principal values of the effective mass tensor are equal, so that the constant energy surfaces are ellipsoids with circular cross-sections (see Figure 6.6). The effective masses of Si and Ge determined by cyclotron resonance are shown in Table 9.1.

9.6 Interband magneto-optics in semiconductors

The application of a magnetic field to a semiconductor splits both the valence and conduction bands into Landau levels, and optical transitions can be induced between hole and electron Landau levels.

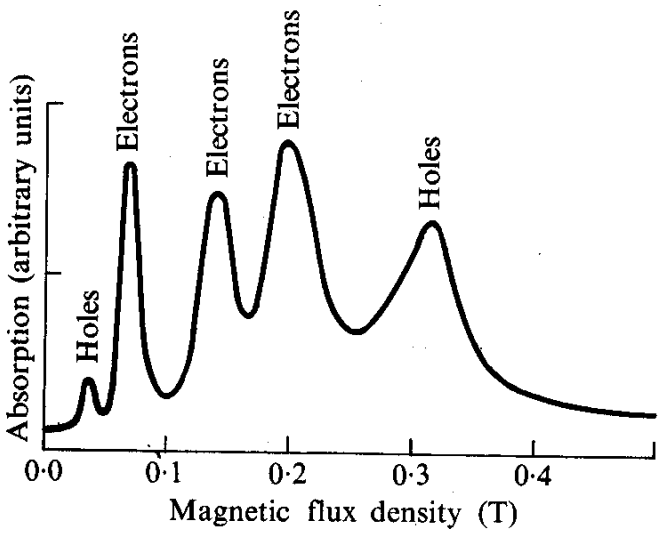

Figure 9.16: Absorption caused by cyclotron resonance of electrons and holes in a single crystal of Ge; the electrons and holes are present because the sample has been illuminated by above-band-gap light. The microwave radiation frequency has been fixed at 24 GHz and the magnetic field, applied in a (110) plane at 60° to a [100] axis, has been swept. Cyclotron resonances due to light (low field) and heavy (high field) holes are visible, as are three electron cyclotron resonances. (Data from Dresselhaus *et al.*, *Phys. Rev.* **98**, 368 (1955).)

In reasonably simple systems, the selection rule for the Landau level index is $\Delta l = 0$; more subtle selection rules apply in materials with complex bandstructures.[16] Taking the former, simpler case, the transitions therefore have the energies

$$E(l,B) = E_g + \frac{\hbar eB}{m^*_{\rm hCR}}(l+\frac{1}{2}) + \frac{\hbar eB}{m^*_{\rm cCR}}(l+\frac{1}{2}), \tag{9.38}$$

where $l = 0, 1, 2, 3..$, and $m^*_{\rm cCR}$ and $m^*_{\rm hCR}$ are the cyclotron masses of the electron and the hole (usually the heavy holes dominate, because of their large density of states) respectively. Such a case is dealt with in the problem sets.

Illustrative experimental data are shown in Figures 9.17 and 9.18. In Figure 9.17, the transmission of a thin film of PbTe has been measured using fixed-frequency radiation of energy $h\nu = 0.2077$ eV as the magnetic field is swept. Transitions between valence-band Landau levels and conduction-band Landau levels are observed as dips in the transmission; note that the dips get further apart and better resolved as the field increases. Equation 9.38 gives a qualitative understanding of these observations; as the field increases, the inter-Landau-level transitions will successively pass through the radiation energy $h\nu$, resulting in a spectrum which looks roughly periodic in $1/B$. PbTe has complex, anisotropic conduction and valence-band extrema, so that the conduction and valence-band Landau level energies vary as the orientation of the magnetic field changes; this is illustrated by the rapid change in the spectra as the sample is tilted in the field, showing how a comprehensive study of this kind can map out the band shapes.

In systems which involve excitonic effects, there are usually complications to be taken into account. Figure 9.18(a) shows the transmission of a GaAs-(Ga,Al)As quantum well at four fixed fields as a function of energy. At zero field, only the excitonic transitions from the hole subbands to the conduction-band subbands are observed, but as the field increases, transitions between the heavy-hole Landau

[16] This is a consequence of the angular momentum carried by the phonon. The valence bands of many semiconductors are based on atomic orbitals with total angular momentum quantum number $J = 3/2$, whereas the conduction band is based on orbitals with $J = 1/2$. Thus the one unit of angular momentum carried by the photon is required to promote an electron across the band gap, leaving nothing to spare to change the Landau-level quantum number l. By contrast, in intraband magneto-optical transitions (cyclotron resonance), the photon's angular momentum is used to change l by one ($\Delta l = \pm 1$).

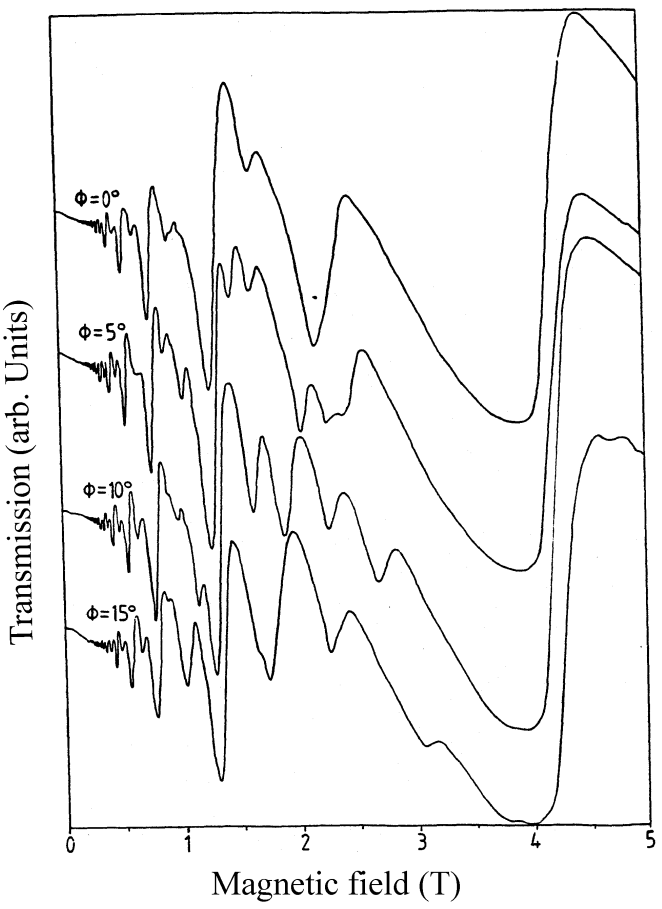

Figure 9.17: Transmission of PbTe at a fixed photon energy of $h\nu = 0.2077$ eV as a function of magnetic field ($T = 1.9$ K). Data for several orientations of the sample in the external field, which is at all times perpendcular to [111], are shown; ϕ is the angle between the magnetic field and $[\bar{1}10]$. (Data from J. Singleton *et al., J. Phys. C: Solid State Phys.* **19**, 77 (1986).)

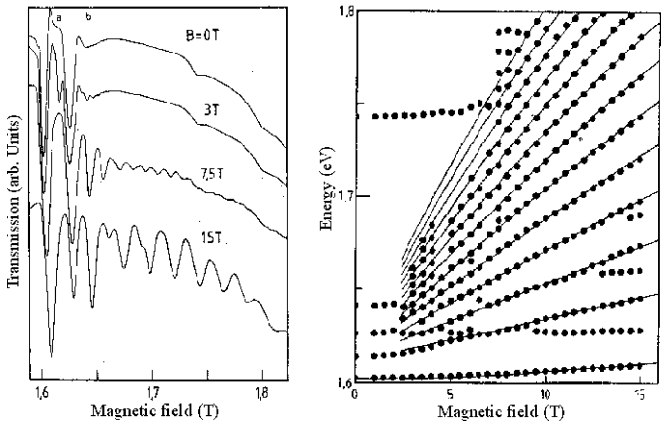

Figure 9.18: (a) Transmission of a 55 ÅGaAs-(Ga,Al)As quantum well at various fixed magnetic fields ($T = 55$ K). The magnetic field has been applied perpendicular to the plane of the quantum well. (b) Resulting fan diagram of transition energies versus magnetic field; points are data, and the lines are a theoretical fit. (From D.C. Rogers *et al., Phys. Rev. B.* **34**, 4002-4009 (1986).)

levels and the conduction-band Landau levels become visible. Figure 9.18 shows a "fan diagram" of the transition energies versus magnetic field for the same sample. Note the following:

- the Landau-level transitions no longer extrapolate back to a point (*c.f.* Equation 9.38), but instead evolve directly from the various states of the exciton (this is particularly notable for the lowest ($l = 0$ and $l = 1$) transitions); there is a one-to-one correspondence between the hydrogen-like levels of the exciton and the Landau level transitions (1s evolves into $l = 0$ transition, 2s evolves into $l = 1$ transition *etc.*;
- the field dependences of the transition energies deviate from straight lines at high energies, curving downwards; this is due to the *non-parabolicity* of the bands as one moves away from the band extrema.

Data such as these can be used to extract the effective masses of the electron and heavy-hole hole subbands, parameters which describe the nonparabolicity and the exciton binding energy.

9.7 Reading

A more detailed treatment of the basic ideas involved in magnetic quantum oscillations is given in *Solid State Physics*, by N.W Ashcroft and N.D. Mermin (Holt, Rinehart and Winston, New York 1976) Chapter 14. Some case studies are given in *Band theory and electronic properties of solids*, by John Singleton (Oxford University Press, 2001) Chapter 8. Simpler descriptions are in *Electrons in Metals and Semiconductors*, by R.G. Chambers (Chapman and Hall, London 1990) Chapter 7, and *Introduction to Solid State Physics*, by Charles Kittel, seventh edition (Wiley, New York 1996) Chapters 8 and 9.

For enthusiasts, a splendid and detailed review of magnetic quantum oscillations in metals is found in *Magnetic oscillations in metals*, by David Shoenberg (Cambridge University Press, Cambridge 1984).